

Near Field Localization via AI-Aided Subspace Methods

Arad Gast, Luc Le Magoarou, and Nir Shlezinger

Abstract—The increasing demands for high-throughput and energy-efficient wireless communications are driving the adoption of extremely large antennas operating at high-frequency bands. In these regimes, multiple users will reside in the radiative near-field, and accurate localization becomes essential. Unlike conventional far-field systems that rely solely on direction of arrival (DoA) estimation, near-field localization exploits spherical wavefront propagation to recover both DoA and range information. While subspace-based methods, such as Multiple Signal Classification (MUSIC) and its extensions, offer high resolution and interpretability for near-field localization, their performance is significantly impacted by model assumptions, including non-coherent sources, well-calibrated arrays, and a sufficient number of snapshots. To address these limitations, this work proposes artificial intelligence (AI)-aided subspace methods for near-field localization that enhance robustness to real-world challenges. Specifically, we introduce *NF-SubspaceNet*, a deep learning-augmented 2D MUSIC algorithm that learns a surrogate covariance matrix to improve localization under challenging conditions, and *DCD-MUSIC*, a cascaded AI-aided approach that decouples angle and range estimation to reduce computational complexity. We further develop a novel model-order-aware training method to accurately estimate the number of sources, that is combined with casting of near field subspace methods as AI models for learning. Extensive simulations demonstrate that the proposed methods outperform classical and existing deep-learning-based localization techniques, providing robust near-field localization even under coherent sources, miscalibrations, and few snapshots.

I. INTRODUCTION

Wireless communications systems are subject to constantly growing demands in terms of throughput, coverage, and energy efficiency. Several emerging technologies are expected to be combined in order to meet these demands [2]. One of the technologies that are envisioned to play a key role in future wireless systems involves employing extremely large [3] and holographic arrays [4] at the base station (BS), using, e.g., large intelligent surfaces [5] and dynamic metasurface antennas [6]. Concurrently, high-frequency bands, such as millimeter waves [7] and sub-THz [8] regimes are expected to be explored in order to utilize their abundant bandwidth.

The combination of extremely large surface based antennas with high frequency signaling gives rise to two considerations: (i) accurate localization of mobile devices becomes essential, allowing BSs to generate the focused beams that are enabled by large surfaces and are crucial at high frequencies [8]; (ii) the Fraunhofer limit can be in the order of over tens of meters [9],

and thus some of the users will likely reside in the *radiative near-field* (termed *near-field* henceforth) [10], [11].

The fact that some of the users are located in the near-field gives rise to passive localization capabilities that are not present in the conventional far-field. While far-field narrowband sources can only be localized in terms of their direction of arrival (DoA), near-field spherical wavefronts allow recovering both DoA and range [12]. Algorithmic tools for localizing multiple near-field sources employ beamforming [13], maximum-likelihood computation [14], compressive sensing techniques [15], [16], cumulant-based schemes [17], [18], null-space projection [19], and covariance-based subspace methods [20]–[26]. The latter family encompasses extensions of the Multiple Signal Classification (MUSIC) algorithm [27] to near-field signals via, e.g., 2D MUSIC [20], [21], multi-stage MUSIC [22]–[25], and iterative 1D MUSIC-type methods [26]. The family of subspace methods is attractive as: (i) the resolution of such algorithms is not dictated by the array geometry; (ii) they naturally support recovering multiple sources; (iii) they are interpretable, in the sense of providing a meaningful spectrum representation; and (iv) they are often simple to implement. However, near-field subspace methods rely on several modeling assumption, e.g., non-coherent sources, calibrated arrays, and many snapshots; when these are violated, performance degrades considerably.

An alternative approach, which does not rely on modeling assumptions, learns to localize from data. Such methods rely on the recent advances in artificial intelligence (AI) tools, and particularly deep learning [28]. Various deep neural networks (DNNs) were suggested for such tasks, including multi-layer perceptrons (MLPs) [29], [30], convolutional neural networks (CNNs) [31]–[38], and attention models [39], [40]. While black-box architectures rely on non-interpretable highly parameterized architectures trained with massive data sets, DNNs can also be combined with classic localization algorithms via model-based deep learning [41]. For far-field DoA recovery, several different augmentations of subspace methods with DNNs were proposed [42]–[49]. These include training DNNs to produce MUSIC spectrum [42], [43], and the usage of DNN models to compute a covariance matrix, either to approach some ground truth clear covariance as in [44]–[46], or to constitute a surrogate covariance for downstream DoA recovery [47]–[49]. The latter approach enables applying subspace methods without being confined to, e.g., coherent sources. However, these existing AI-aided methods are geared towards far-field sources, and rely on differentiable DoA estimation, which does not extend to the near-field.

This work proposes AI-aided methods that learn to perform subspace-based near-field localization. We aim to preserve the interpretable operation of subspace near-field localizers, and particularly the ability to obtain an informative eigen and MUSIC spectra that enable identifying the number of sources and their location, while coping with coherent sources,

Parts of this work were presented at the IEEE International Conference on Acoustics, Speech, and Signal Processing (ICASSP) 2025 as the paper [1]. A. Gast and N. Shlezinger are with the School of ECE, Ben-Gurion University of the Negev, Be'er-Sheva, Israel (e-mails: gast@post.bgu.ac.il; nirshl@bgu.ac.il). L. Le Magoarou is with Univ. Rennes, INSA Rennes, CNRS, IETR-UMR 6164, France (e-mail: luc.Le-magoarou@insa-rennes.fr). The work was supported by the European Research Council (ERC) under the ERC starting grant nr. 101163973 (FLAIR), the Israel Innovation Authority, and the French national research agency, grant ANR-23-CE25-0013.

miscalibrations, and few snapshots.

Our main contributions are summarized as follows:

- **AI-Aided Near-Field MUSIC:** We propose a deep learning-aided extension of 2D near-field MUSIC, termed *NF-SubspaceNet*. Our method follows the general methodology of SubSpaceNet [49], which learns to produce a surrogate covariance matrix tailored for subspace-based localization. However, SubSpaceNet relies on the differentiability of far-field estimators such as Root-MUSIC during training, which are not applicable in the near-field setting. To enable end-to-end training in this more challenging regime, we introduce a differentiable loss function inspired by [50], which supervises the MUSIC spectrum itself rather than the final estimated parameters, thus avoiding the need for differentiable post-processing.
- **Reduced Complexity Cascaded Algorithm:** As 2D MUSIC, either model-based or AI-aided, involves a two-dimensional grid search that can be computationally intensive, we propose an alternative reduced complexity algorithm termed *deep-learning-aided cascaded differentiable MUSIC* (*DCD-MUSIC*). DCD-MUSIC is based on Estimation of signal parameters via rotational invariance techniques (ESPRIT)-MUSIC cascade [24], decomposing DoA and range recovery, leveraging the differentiability of ESPRIT to train a dedicated DNN to compute a surrogate far-field covariance, used to recover the DoAs. We then propose a soft-to-hard approximation of MUSIC to train another DNN to produce a covariance for range recovery via 1D MUSIC for each DoA.
- **Model-Order-Aware Training Method:** We introduce a novel training scheme that combines the accuracy in localizing the sources with the need to *identify the number of sources*. We specifically propose three different training loss terms that balance the ability to recover the number of sources from the surrogate eigenspectrum via conventional thresholding, as well as model-order selection techniques based on Minimum Description Length (MDL) [51] and Akaike Information Criterion (AIC) [52].
- **Extensive Experimentation:** We provide a detailed qualitative and quantitative evaluation of our algorithms. For the latter, we contrast our AI-aided methods with representative model-based and data-driven near-field localization methods. We demonstrate that our methods outperform various benchmarks and localize multiple near-field as well as far-field coherent sources in challenging settings while providing a meaningful and interpretable spectrum.

The rest of this paper is organized as follows: Section II formulates the near field localization setup, and briefly reviews relevant subspace methods. Section III presents our AI-aided near-field localization methods, that are numerically evaluated in Section IV, while Section V provides concluding remarks.

Throughout this paper, we use boldface lower-case and upper-case letters for vectors (e.g., \mathbf{x}) and matrices (e.g., \mathbf{X}), respectively. The n th entry of \mathbf{x} is denoted by $[\mathbf{x}]_n$. Calligraphic letters denote sets, e.g., \mathcal{X} , with \mathbb{C} being the set of complex numbers, while $\|\cdot\|$, $\mathbf{1}_{(\cdot)}$, $(\cdot)^T$, and $(\cdot)^H$ are the ℓ_2 norm, indicator function, transpose, and conjugate transpose, respectively.

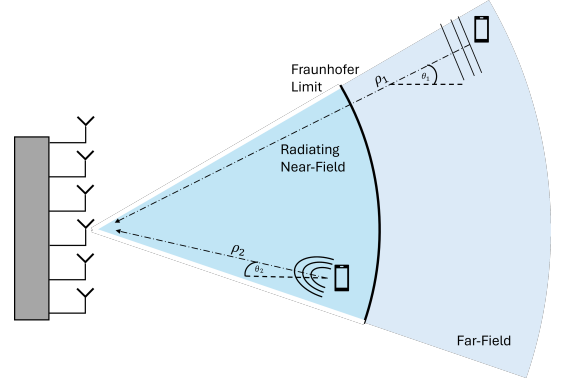


Fig. 1: Multi source localization illustration.

II. SYSTEM MODEL AND PRELIMINARIES

This section formulates near-field localization and reviews necessary preliminaries. We first describe the signal model in Subsection II-A and the localization problem in Subsection II-B. Then, we briefly review background in model-based and data-driven Subspace methods in Subsection II-C.

A. Signal Model

The conventional modeling for passive localization in two-dimensional space considers M narrowband sources impinging an uniform linear array (ULA). The ULA has $N > M$ elements, that are separated with spacing d . We write the angle and distance of the m th source from the array as θ_m and ρ_m , respectively. We focus on settings where the sources possibly lie in the *radiative near-field* [10], namely, the distance of the m th source, ρ_m , can be between the Fresnel limit and the Fraunhofer limit of the array. For wavelength λ and array aperture $D = (N - 1) \cdot d$, this implies that [53]

$$\sqrt[3]{D^4/8\lambda} < \rho_m < 2 \cdot D^2/\lambda, \quad \forall m \in \{1, \dots, M\}. \quad (1)$$

If the distance is larger than the Fraunhofer limit $2 \cdot D^2/\lambda$, then the source is said to lie in the *far-field*, which is the conventional regime considered in DoA estimation settings [54]. The considered system is illustrated in Fig. 1.

The signal received at the array at time instant t is described as the $N \times 1$ vector $\mathbf{x}(t)$, given by:

$$\mathbf{x}(t) = \sum_{m=1}^M \mathbf{a}(\theta_m, \rho_m) s_m(t) + \mathbf{w}(t). \quad (2)$$

In (2), $s_m(t)$ is the m th source signal, $\mathbf{w}(t)$ is an additive noise, and $\mathbf{a}(\theta, \rho)$ is the steering vector towards (θ, ρ) . The common approach to model the near-field steering vector, adopted in [17]–[25], writes its n th element as

$$[\mathbf{a}(\theta_m, \rho_m)]_n = e^{jn\omega(\theta_m) + jn^2\psi(\theta_m, \rho_m)}, \quad (3)$$

for $n \in \{1, \dots, N\}$, where

$$\omega(\theta_m) \triangleq -\frac{2\pi}{\lambda} d \sin(\theta_m), \quad \psi(\theta_m, \rho_m) \triangleq \frac{\pi}{\lambda} \frac{d^2 \cos^2(\theta_m)}{\rho_m}.$$

An alternative model proposed in [55] formulates the elements of the near-field steering vector as

$$[\mathbf{a}(\theta_m, \rho_m)]_n = \frac{\rho_m}{\rho_{n,m}} e^{jn\omega(\theta_m) + jn^2\psi(\theta_m, \rho_m)}, \quad (4)$$

where $\rho_{n,m}$ is the distance of the m th source to the n th sensor element in the array. When ρ_m is larger than the Fraunhofer limit, it holds that $\psi(\theta_m, \rho_m) \approx 0$ and $\rho_{n,m} \approx \rho_m$, and thus both (3) and (4) reduce to the conventional ULA far-field steering vector representation [54].

The signal model in (2) is defined for a single snapshot. Gathering the signals over T snapshots yields a matrix signal model, which holds for both formulations of the steering vector. Letting $\boldsymbol{\theta} \triangleq [\theta_1, \dots, \theta_M]^T$, $\boldsymbol{\rho} \triangleq [\rho_1, \dots, \rho_M]^T$, the matrix model is given by

$$\mathbf{X} = \mathbf{A}(\boldsymbol{\theta}, \boldsymbol{\rho})\mathbf{S} + \mathbf{W}, \quad (5)$$

where $\mathbf{A}(\boldsymbol{\theta}, \boldsymbol{\rho}) \in \mathbb{C}^{N \times M}$ is the steering matrix whose m th column is $\mathbf{a}(\theta_m, \rho_m)$; while $\mathbf{S} \triangleq [\mathbf{s}(1), \dots, \mathbf{s}(T)] \in \mathbb{C}^{M \times T}$, $\mathbf{X} \triangleq [\mathbf{x}(1), \dots, \mathbf{x}(T)] \in \mathbb{C}^{N \times T}$, and $\mathbf{W} \triangleq [\mathbf{w}(1), \dots, \mathbf{w}(T)] \in \mathbb{C}^{N \times T}$.

B. Problem Formulation

We wish to localize the sources, namely, estimate $\boldsymbol{\theta}$ and $\boldsymbol{\rho}$ from the measured \mathbf{X} . The number of sources M is not known a-priori, but is assumed to be smaller than N . Accordingly, we are interested in an algorithm that maps \mathbf{X} into an estimate of the number of sources $\hat{M} \in \{0, 1, \dots, N-1\}$ as well as the corresponding estimates of the angles and ranges, respectively denoted as

$$\hat{\boldsymbol{\theta}} \in [-\pi/2, \pi/2]^{\hat{M}}, \quad \hat{\boldsymbol{\rho}} \in [\sqrt{D^4/8\lambda}, 2 \cdot D^2/\lambda]^{\hat{M}}.$$

Recall that for conventional far-field localization, i.e., when ρ_m is larger than the Fraunhofer limit in (1), then the distance cannot be recovered from \mathbf{X} . Accordingly, a range of $[\hat{\rho}]_m = 2 \cdot D^2/\lambda$ estimates that the source as lying in the far-field.

Unlike conventional approaches for localizing in the near-field [17]–[25], we focus on challenging settings, where, e.g.,

- C1** The sources are coherent, i.e., the covariance matrix of $\mathbf{s}(t)$, denoted \mathbf{R}_S , is non-diagonal.
- C2** The array includes unknown mis-calibrations, e.g., the actual element spacing may differ from the value of d provided to the algorithm, and may deviate from $\frac{\lambda}{2}$.
- C3** The number of snapshots T is small, and the signal-to-noise ratio (SNR) is low.

As follows from our formulation of the setup, we are also interested in coping with the following challenge:

- C4** Each source can be either in the far-field or in the near-field.

To tackle these possible issues, we assume access to labeled data, obtained from, e.g., simulations or field measurements. The data is comprised of J pairs of observation and their angles-ranges, denoted as

$$\mathcal{D} = \left\{ (\mathbf{X}_j, \{(\theta_{m,j}, \rho_{m,j})\}_{m=1}^{M_j}) \right\}_{j=1}^J. \quad (6)$$

C. Model-Based and Data-Driven Subspace Methods

1) *Subspace Methods*: A leading family of algorithms for passive localization is that of *subspace methods* [54, Ch. 2]. These methods localize multiple sources in the absence of **C1-C3** by extracting from the input covariance orthogonal representations of the signal and noise subspaces. In doing so, they can localize with resolution that is not dictated by the geometry of the ULA.

Specifically, for non-coherent sources (not meeting **C1**), the eigenvalues decomposition (EVD) of the covariance of $\mathbf{x}(t)$ contains M dominant eigenvalues, whose eigenvectors correspond to the signal subspace. The remaining $N - M$ eigenvectors, denoted by $N \times (N - M)$ matrix \mathbf{U}_W , represent the noise subspace and are orthogonal to the steering vectors [27], i.e.,

$$\|\mathbf{U}_W^H \mathbf{a}(\theta_m, \rho_m)\| = 0, \quad \forall m \in \{1, \dots, M\}. \quad (7)$$

Subspace methods first estimate the input covariance as $\hat{\mathbf{R}}_X = \frac{1}{T} \sum_{t=0}^{T-1} \mathbf{x}(t) \mathbf{x}^H(t)$, requiring sufficient snapshots (not meeting **C3**) to estimate it. The number of sources \hat{M} and noise subspace $\hat{\mathbf{U}}_W$ are estimated from the EVD of $\hat{\mathbf{R}}_X$, by dividing its eigenvalues, denoted $\{\hat{\lambda}_n\}$, into \hat{M} dominant and $N - \hat{M}$ least dominant ones (noise subspace). Specifically, the setting of \hat{M} is often realized via *thresholding*, i.e., by comparing to a fixed threshold Λ and setting

$$\hat{M} = \sum_{n=1}^N \mathbf{1}_{\hat{\lambda}_n > \Lambda}. \quad (8)$$

An alternative approach treats the setting of M using *model-order selection* tests, such as the *MDL* criterion [51] (which can be viewed as an approximation of the Bayesian Information criterion) or the *AIC* [52]. Assuming that the signals $\mathbf{s}(t)$ and the noise $\mathbf{w}(t)$ are i.i.d. Gaussian, such tests estimate M under the signal model in (2) as [56]

$$\begin{aligned} \hat{M} = \arg \min_{M \in \{0, \dots, N-1\}} & -T \sum_{n=M+1}^N \log(\hat{\lambda}_n) \\ & + T(N - M) \log \left(\frac{1}{N - M} \sum_{n=M+1}^N \hat{\lambda}_n \right) \\ & + \frac{1}{2} (2M(N - M) + 1) \cdot \zeta(T), \end{aligned} \quad (9)$$

with $\zeta(t) = \log(T)$ for MDL, and $\zeta(T) \equiv 2$ for AIC.

2) *Near-Field MUSIC*: Once \hat{M} and the noise subspace $\hat{\mathbf{U}}_W$ are recovered, subspace methods localize the sources based on the property in (7). When the sources lie in the far-field, and thus the ULA steering vector models linear phase accumulation, the angles $\boldsymbol{\theta}$ can be estimated based on (7) using different algorithms, including MUSIC [27], Root-MUSIC [57], and ESPRIT [58].

While Root-MUSIC and ESPRIT are particularly tailored for far-field sources, MUSIC can be applied regardless of the steering matrix structure, and can thus be extended for near-field localization [20]. Specifically, Near-Field MUSIC estimates $\boldsymbol{\theta}$ and $\boldsymbol{\rho}$ by finding the \hat{M} peaks in the MUSIC spectrum, given by

$$P_{\text{MUSIC}}(\boldsymbol{\theta}, \boldsymbol{\rho}) = \|\hat{\mathbf{U}}_W^H \mathbf{a}(\boldsymbol{\theta}, \boldsymbol{\rho})\|^{-2}. \quad (10)$$

The MUSIC spectrum in (10) visually represents the location of the sources. It is computed by expressing the steering vectors via (3) (which can be inaccurate under **C2**). Finding the peaks of (10) typically requires searching over a 2D grid.

3) *SubspaceNet*: As detailed above, subspace methods are typically studied in the context of far-field DoA recovery. There, it was recently shown in [49] that one can incorporate deep learning techniques to make subspace methods operate in the presence of Challenges **C1-C3**.

Specifically, the SubspaceNet algorithm of [49] suggested to train a DNN to map the observed signal \mathbf{X} into a *surrogate* covariance matrix that is useful for downstream subspace-based DoA recovery, as if **C1-C3** are not present. This was achieved by, drawing inspiration from focusing methods [59], first extracting the autocorrelation features as

$$\mathbf{R}_x[\tau] = \frac{1}{T-\tau} \sum_{t=0}^{T-\tau} \mathbf{x}(t)\mathbf{x}^H(t+\tau), \quad (11)$$

for $\tau \in 0, \dots, \tau_{\max}$. The autocorrelation features, $\{\mathbf{R}_x[\tau]\}_{\tau=0}^{\tau_{\max}}$, are then mapped into real-valued features by concatenating the real and imaginary parts, and processing the resulting tensor through a de-noising CNN auto-encoder with trainable parameters ψ . The network outputs are the real and imaginary parts of an $N \times N$ matrix $\mathbf{K}(\mathbf{X}; \psi)$, used to obtain a positive definite surrogate covariance via

$$\hat{\mathbf{R}}(\mathbf{X}; \psi) = \mathbf{K}(\mathbf{X}; \psi)\mathbf{K}^H(\mathbf{X}; \psi) + \epsilon \mathbf{I}_N, \quad \epsilon > 0. \quad (12)$$

The training procedure evaluated the surrogate covariance in (12) based on its usefulness for downstream subspace based DoA estimation. This was achieved by providing $\hat{\mathbf{R}}(\mathbf{X}; \psi)$ to a *differentiable* far-field subspace method (particularly ESPRIT and Root-MUSIC). Leveraging the differentiability of the subsequent far-field subspace method, the internal DNN was trained to minimize the DoA estimation error on a training dataset, where the gradients of the empirical risk were computed by backpropagating through the subspace method [49].

III. AI-AIDED SUBSPACE METHODS

The fact that far-field AI-augmented subspace methods rely on using a differentiable subspace method during training, and particularly ESPRIT or Root-MUSIC, implies that these far-field algorithms do not extend to the radiating near-field. However, their underlying concept, advocating the usage of deep learning techniques to learn surrogate covariance matrices for subspace-based localization purposes, guides us in next proposing AI-aided near-field subspace methods.

Accordingly, in this section, we present two such algorithms: The first, termed *NF-SubspaceNet* (presented in Subsection III-A), extends the methodology of (far-field) SubspaceNet to Near-Field MUSIC; it does so by integrating novel tools to evaluate the resulting spectrum while facilitating accurate estimation of the number of sources. Our second algorithm, coined *DCD-MUSIC* (presented in Subsection III-B), adopts a different approach, where instead of modifying the localization algorithm to be near-field oriented, we transform the signal covariance to correspond to far-field signals. This is achieved by decoupling angle and range recovery in a cascaded fashion, drawing inspiration from [24], [60]. We conclude with a qualitative comparison and a discussion in Subsection III-C.

A. NF-SubspaceNet

1) *Rationale*: As discussed in Subsection II-C3, it was shown in [49] that the availability of data as in (6) can be utilized to enable subspace methods to operate under challenges **C1-C3**, by

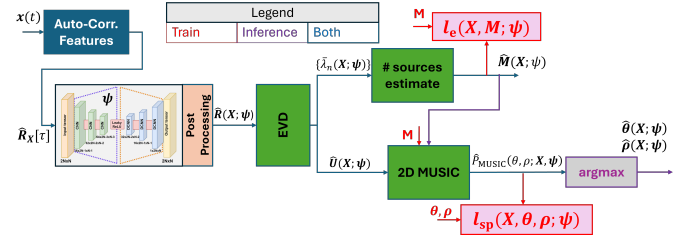


Fig. 2: NF-SubspaceNet illustration.

training a dedicated DNN to map the observations in to a surrogate covariance matrix. However, directly extending this methodology to near-field scenarios (as well as to mixed near-field/far-field **C4**) is not straightforward. This limitation arises because the differentiable algorithms underpinning the training of the DNN (ESPRIT or Root-MUSIC) are incompatible with the fact that the phase of the entries of the steering matrix is a non-linear function of the antenna index in the near-field. The subspace method that is suitable in the near-field, i.e., Near-Field MUSIC, is not differentiable due to its reliance on a peak-finding operation.

To overcome these challenges, we leverage recent developments in differentiable approximations of MUSIC-type algorithms [50]. Specifically, we allow SubspaceNet to be applied for localizing mixed near-field and far-field sources by proposing a novel loss function, that evaluates the covariance based on two main criteria: (i) its usefulness for producing a meaningful *near-field MUSIC spectrum* (as opposed to predicting the correct locations as in previous AI-augmented subspace methods). This is achieved by encouraging the noise subspace to be as orthogonal as possible to the steering matrix at the true source locations; and (ii) the *distinguishability of its eigenspectrum* into signal and noise subspaces.

2) *Architecture*: Following the above rationale, we design NF-SubspaceNet to employ a dedicated DNN with trainable parameters ψ , whose input is the (complex-valued) autocorrelation features $\{\mathbf{R}_x[\tau]\}_{\tau=0}^{\tau_{\max}}$, computed via (11). The outputs of the DNN are the real and imaginary parts that form the $N \times N$ matrix $\mathbf{K}(\mathbf{X}; \psi)$, which in turn is converted into the surrogate covariance $\hat{\mathbf{R}}(\mathbf{X}; \psi)$. Hence, the DNN maps a $2(\tau_{\max} + 1) \times N \times N$ tensor into a $2 \times N \times N$ tensor.

We use an architecture comprised of a sequence of convolutional layers followed by a sequence of deconvolutional layers as a form of an autoencoder (with non identical input and output dimensions). Drawing inspiration from [61], we employ anti-rectifier activations to avoid sparsification of the internal features while preserving the simplicity of conventional ReLU. Instead of using (12) to directly obtain the surrogate covariance as in [49], we introduce a normalization layer whose purpose is to regularize the variation in the eigenvalues, that play a key role in identifying the number of sources. To that aim, we normalize (12) by its largest eigenvalue, i.e., its *spectral norm*, and thus the surrogate covariance is obtained as

$$\hat{\mathbf{R}}(\mathbf{X}; \psi) = \frac{\mathbf{K}(\mathbf{X}; \psi)\mathbf{K}^H(\mathbf{X}; \psi) + \epsilon \mathbf{I}_N}{\|\mathbf{K}(\mathbf{X}; \psi)\mathbf{K}^H(\mathbf{X}; \psi) + \epsilon \mathbf{I}_N\|_2}. \quad (13)$$

The last layer of the architecture is a learnable skip connection with a learnable parameter α , which is constrained to the range (0, 1). This parameter introduces a correction term to

the empirical covariance of the input signal, $\mathbf{R}_x[\tau = 0]$, by defining the surrogate covariance as follows:

$$\hat{\mathbf{R}}(\mathbf{X}; \psi) = \hat{\mathbf{R}}(\mathbf{X}; \psi) + \alpha \mathbf{R}_x[\tau = 0].$$

During inference, the surrogate covariance matrix is processed with Near-Field MUSIC for angle and range estimation. First, the eigenvalues of $\hat{\mathbf{R}}(\mathbf{X}; \psi)$ are used to identify the number of sources \hat{M} via either (8) or (9). Next, the $N \times \hat{M}$ noise subspace is computed from $\hat{\mathbf{R}}(\mathbf{X}; \psi)$, and is used to formulate the MUSIC spectrum, denoted $P_{\text{MUSIC}}(\theta, \rho; \mathbf{X}, \psi)$, using (10). Then, the locations are recovered from the \hat{M} peaks of $P_{\text{MUSIC}}(\theta, \rho; \mathbf{X}, \psi)$. Sources located at the upper limit of the ρ range are labeled as far-field sources. The procedure is summarized as Algorithm 1, and illustrated in Fig. 2.

Algorithm 1: NF-SubspaceNet Localization

Init: Trained DNN ψ ; hyperparameters (ϵ, τ_{\max})

Input: Observations \mathbf{X}

- 1 Compute $\{\mathbf{R}_x[\tau]\}_{\tau=0}^{\tau_{\max}}$ via (11);
 - 2 Apply DNN and (13) to get $\hat{\mathbf{R}}(\mathbf{X}; \psi)$;
 - 3 Set $\{\bar{\lambda}_n(\mathbf{X}; \psi)\}$ as eigenvalues of $\hat{\mathbf{R}}(\mathbf{X}; \psi)$;
 - 4 Compute \hat{M} from $\{\bar{\lambda}_n(\mathbf{X}; \psi)\}$ via (8) or (9);
 - 5 Formulate spectrum $P_{\text{MUSIC}}(\theta, \rho; \mathbf{X}, \psi)$, using (10);
 - 6 Set $\hat{\theta}, \hat{\rho}$ as \hat{M} peaks of $P_{\text{MUSIC}}(\theta, \rho; \mathbf{X}, \psi)$;
 - 7 **return** $\hat{\theta}, \hat{\rho}$
-

3) *Training:* The learning procedure, i.e., the setting of the trainable parameters ψ from the dataset \mathcal{D} , aims at having NF-SubspaceNet produce accurate predicted locations based on the signals in \mathcal{D} . While presumably one would wish to do so by converting NF-SubspaceNet into a trainable discriminative machine learning model [62], following the conventional approach in model-based deep learning [41], such an approach cannot be carried out directly, as gradients cannot propagate through the near-field MUSIC algorithm. To overcome this challenge we introduce a novel loss function that (i) evaluates the near-field MUSIC spectrum *prior to peak finding*; and (ii) encourages accurate recovery of the number of sources via thresholding or model-order selection tests.

Spectrum Loss: To evaluate localization accuracy, we formulate a loss inspired by the core principles of subspace methods. Instead of computing the loss based on the predicted source locations, we seek orthogonality of the noise subspace to the steering matrix. This is achieved by encouraging the surrogate covariance to produce a near-field MUSIC spectrum whose inverse is minimized at the sources' locations, namely,

$$l_{\text{sp}}(\mathbf{X}, \theta, \rho; \psi) = \sum_{m=1}^M P_{\text{MUSIC}}^{-1}(\theta_m, \rho_m; \mathbf{X}, \psi). \quad (14)$$

By minimizing (14), the surrogate covariance matrix is optimized to yield a noise subspace that is highly orthogonal to the steering matrix at the source positions.

Model-Order Loss: We design a regularization component to foster a more distinct eigenspectrum, and particularly, enhance the ability to recover M from the (sorted) eigenvalues of the surrogate covariance $\hat{\mathbf{R}}(\mathbf{X}; \psi)$, denoted by $\{\bar{\lambda}_n(\mathbf{X}; \psi)\}_{n=1}^N$.

In order to tailor the loss term to the downstream method for detecting M , we propose either of the following formulations:

- *Thresholding:* When the subspace method recovers M via (8), we propose to penalize the weights ψ to yield an eigenspectrum where the M th eigenvalue is misclassified as noise or the $M + 1$ th eigenvalue is misclassified as a signal. The proposed regularization term is

$$l_e(\mathbf{X}, M; \psi) = \prod_{m=M}^{M+1} (\bar{\lambda}_m(\mathbf{X}; \psi) - \Lambda). \quad (15)$$

Λ here is treated as a hyperparameter.

- *Model-Order Selection Test:* When M is recovered during inference using a model-order selection test, e.g., MDL or AIC as in (9), we use the explicit test as a loss term, encouraging the model to minimize it at the true number of sources. Accordingly, the regularization term is comprised of the terms (9) that depend on ψ_a , i.e.,

$$l_e(\mathbf{X}, M; \psi) = \frac{-1}{N-M} \sum_{n=M+1}^N \log(\bar{\lambda}_n(\mathbf{X}; \psi)) + \log\left(\frac{1}{N-M} \sum_{n=M+1}^N \bar{\lambda}_n(\mathbf{X}; \psi)\right). \quad (16)$$

Training Algorithm: The overall loss function used for training NF-SubspaceNet based on a dataset \mathcal{D} is given by

$$\mathcal{L}_{\mathcal{D}}(\psi) = \frac{1}{|\mathcal{D}|} \sum_{j=1}^{|\mathcal{D}|} l_{\text{sp}}(\mathbf{X}_j, \theta_j, \rho_j; \psi) + \mu_e l_e(\mathbf{X}_j, M_j; \psi), \quad (17)$$

where $\mu_e > 0$ is a regularization coefficient, balancing the spectrum loss with the model-order loss. The selection of (14) allows training Algorithm 2 as a machine learning architecture using conventional first-order optimizers, since it enables gradient propagation through each step of the algorithm (see Fig. 2). The complete processing chain from the empirical autocorrelation features to the near-field MUSIC spectrum, which includes traditional CNN layers, as well as differentiable operations like EVD (see, e.g., [63]) and tensor multiplications, is end-to-end differentiable. The training procedure, based on mini-batch stochastic gradient descent (SGD), is summarized in Algorithm 2.

Algorithm 2: SGD Training of NF-SubspaceNet

Init: Learning parameters (μ, e_{\max}, B) ,

hyperparameters (ϵ, τ_{\max}) , initial weights ψ ;

Input: Training dataset \mathcal{D}

- 1 **for** $e = 1, \dots, e_{\max}$ **do**
 - 2 Randomly divide \mathcal{D} into B batches;
 - 3 **for each batch** $\mathcal{D}^{(b)}$ **do**
 - 4 Compute $\hat{\mathbf{R}}(\mathbf{X}_j^{(b)}; \psi)$, $\forall \mathbf{X}_j^{(b)} \in \mathcal{D}^{(b)}$;
 - 5 Compute loss $\mathcal{L}_{\mathcal{D}^{(b)}}(\psi)$ using (17);
 - 6 Update parameters $\psi \leftarrow \psi - \mu \nabla_{\psi} \mathcal{L}_{\mathcal{D}^{(b)}}(\psi)$;
 - 7 **return** ψ
-

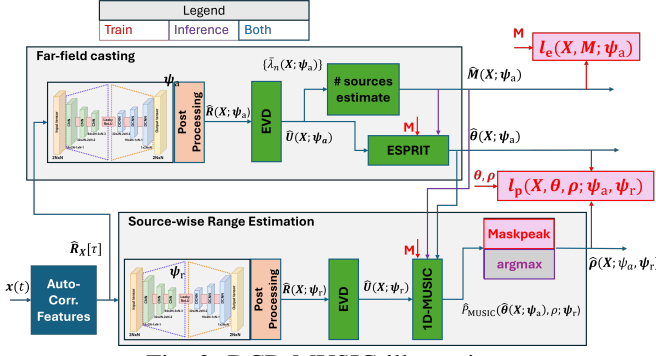


Fig. 3: DCD-MUSIC illustration.

B. DCD-MUSIC

1) *Rationale*: The formulation of NF-SubspaceNet in Subsection III-A aims at modifying existing far-field AI-aided subspace methods (and particularly SubspaceNet), to be applicable with near-field subspace methods. In doing so, NF-SubspaceNet inherits some of the shortcomings of these classical methods, e.g., the need to apply a 2D search over the MUSIC spectrum during inference, whose granularity limits resolution. Here, we derive an alternative scheme, coined DCD-MUSIC, that follows an opposite line-of-thought: instead of modifying the subspace method from far-field to near-field, as in NF-SubspaceNet, it *recasts the signal statistics as originating from far-field sources*, with which far-field AI-aided subspace methods can be applied.

Specifically, the design of DCD-MUSIC is motivated by two key observations: (i) 2D MUSIC variants (e.g., Near-Field MUSIC) can often be approached, with reduced complexity, by a cascade of ESPRIT and one-dimensional MUSIC, each applied along a distinct search coordinate [24], [60]; (ii) as demonstrated in [49], DNN-based covariance pre-processing can enable interpretable far-field subspace methods to recover DoA in scenarios where signals deviate from ideal far-field models. Building on these insights, DCD-MUSIC performs near-field localization using a two-stage process, which first produces a far-field surrogate covariance for angle recovery, after which the range for each source is separately recovered.

2) *Architecture*: As outlined above, DCD-MUSIC is comprised of two modules: *Far-Field Casting*, and *Source-Wise Range Estimate*. We next elaborate on each of these stages, with the overall two-stage process is depicted Fig. 3.

Far-Field Casting: First, a DNN-based subspace-oriented surrogate covariance extraction transforms the signal into a far-field representation. The far-field surrogate covariance is used to estimate number of sources, M , and their angles, θ .

Specifically, we employ the DNN architecture detailed in Subsection III-A with parameters ψ_a . The DNN learns to map the input \mathbf{X} into a surrogate covariance denoted $\hat{\mathbf{R}}(\mathbf{X}; \psi_a)$, that is amenable to far-field subspace extraction of M and θ . The former is carried out using either thresholding (8) or model-order selection tests (9) (neither of which was included in the formulation of SubspaceNet in [49], and is adopted from NF-SubspaceNet). The angles of the sources are estimated from the covariance as $\hat{\theta}(\mathbf{X}; \psi_a)$ using ESPRIT.

Source-Wise Range Estimate: Having estimated M as $\hat{M}(\mathbf{X}; \psi_a)$ and θ as $\hat{\theta}(\mathbf{X}; \psi_a)$, we proceed to recover ρ . This

is achieved by searching the MUSIC spectrum for a peak for each estimated $\hat{\theta}_m(\mathbf{X}; \psi_a)$. Since we wish to cope with **C1-C3**, we cannot directly apply MUSIC to the empirical covariance, and should again seek a surrogate covariance using a DNN. Unlike the DNN ψ_a , here the surrogate covariance is not required to represent far-field signaling. Thus, a dedicated CNN autoencoder with parameters ψ_r is used. Its output, denoted $\hat{\mathbf{R}}(\mathbf{X}; \psi_r)$, is obtained using similar processing to those in (13).

The surrogate covariance is then used $\hat{M}(\mathbf{X}; \psi_a)$ times, for estimating the ranges of the sources for each of the estimated angles using one-dimensional MUSIC. Accordingly, by letting $\hat{\mathbf{U}}_W(\mathbf{X}; \psi_r, \psi_a)$ be the $N - \hat{M}(\mathbf{X}; \psi_a)$ least dominant eigenvectors of $\hat{\mathbf{R}}(\mathbf{X}; \psi_r)$, we estimate $\hat{\rho}_m(\mathbf{X}; \psi_r, \psi_a)$ via

$$\arg \max_{\rho} \|\hat{\mathbf{U}}_W^H(\mathbf{X}; \psi_r, \psi_a) \mathbf{a}(\hat{\theta}_m(\mathbf{X}; \psi_a), \rho)\|^{-2}, \quad (18)$$

for each $m \in \{1, \dots, \hat{M}(\mathbf{X}; \psi_a)\}$. The arg max operation in (18) is computed by grid search over a range holding (1). Sources at the far edge of the range, i.e., at the limit, are labeled as far-field sources. The resulting DCD-MUSIC algorithm is summarized as Algorithm 3. The chosen configuration employs ESPRIT for angle estimation followed by MUSIC for range recovery. While alternative designs are possible, such as using Root-MUSIC for angle estimation combined with a spectrum-based loss for range, instead of approximation of the peak finding operation, we opt the ESPRIT-MUSIC configuration with mask-peak based on empirical trials across our evaluated scenarios.

Algorithm 3: DCD-MUSIC Localization

Init: Trained DNNs ψ_r, ψ_a ; hyperparameters (ϵ, τ_{\max}) .
Input: Observations \mathbf{X} ;
1 Apply DNNs to \mathbf{X} to obtain $\hat{\mathbf{R}}(\mathbf{X}; \psi_a), \hat{\mathbf{R}}(\mathbf{X}; \psi_r)$;
2 Set $\{\bar{\lambda}_n(\mathbf{X}; \psi_a)\}$ as eigenvalues of $\hat{\mathbf{R}}(\mathbf{X}; \psi_a)$;
3 Compute \hat{M} from $\{\bar{\lambda}_n(\mathbf{X}; \psi_a)\}$ via (8) or (9);
4 Estimate $\hat{\theta}$ from $\hat{\mathbf{R}}(\mathbf{X}; \psi_a)$ via far-field ESPRIT;
5 **for** $m = 1, \dots, \hat{M}$ **do**
6 Estimate $\hat{\rho}_m$ via (18);
7 **return** $\hat{\theta}, \hat{\rho}$

3) *Training*: We train DCD-MUSIC, namely, set ψ_a, ψ_r from the data \mathcal{D} in (6), in three sequential steps, designed to gradually tune each of the modules of DCD-MUSIC. These training stages are termed *Angle*, *Range*, and *Position Training*.

Angle Training: We first train only ψ_a by evaluating $\hat{\mathbf{R}}(\mathbf{X}; \psi_a)$ based on (i) its usefulness for angle recovery via the (differentiable) far-field ESPRIT; and (ii) the accuracy of the recovered number of sources.

To evaluate angle recovery, we use the root mean squared periodic error (RMSPE) loss, which accounts for the periodic nature of the angles [64]. This loss term is given by

$$l(\mathbf{X}, \theta; \psi) = \min_{\mathbf{P} \in \mathcal{P}_M} \frac{\|\text{mod}_{\pi}(\theta - \mathbf{P}\hat{\theta}(\hat{\mathbf{R}}(\mathbf{X}; \psi)))\|}{\sqrt{M}}, \quad (19)$$

whereas \mathcal{P}_M be the set $M \times M$ permutation matrices, and mod_{π} denote modulo π . To encourage accurate recovery of M , we

employ the model-order loss detailed in Subsection III-A. Thus, the overall loss term used for training ψ_a over the dataset \mathcal{D} is

$$\mathcal{L}_{\mathcal{D}}^a(\psi_a) = \frac{1}{|\mathcal{D}|} \sum_{j=1}^{|\mathcal{D}|} l_a(\mathbf{X}_j, \boldsymbol{\theta}_j; \psi_a) + \mu_e l_e(\mathbf{X}_j, M_j; \psi_a), \quad (20)$$

where $\mu_e > 0$ is a regularization coefficient.

Range Training: The second step trains ψ_r using the input and the angles $\hat{\boldsymbol{\theta}}$ recovered by the trained ψ_a . Unlike the estimation of far-field angles, range recovery cannot be carried out using differentiable subspace methods (ESPRIT or Root-MUSIC) even if none of C1-C4 hold, due to its nonlinear phase accumulation. Accordingly, we apply one-dimensional MUSIC for each angle $\hat{\theta}_m(\mathbf{X}; \psi_a)$, using the surrogate covariance $\hat{\mathbf{R}}(\mathbf{X}; \psi_r)$ and the steering vectors $\mathbf{a}(\hat{\theta}_m(\mathbf{X}; \psi_a), \rho)$, to estimate the distance as $\hat{\rho}_m(\hat{\mathbf{R}}(\mathbf{X}; \psi_r), \hat{\boldsymbol{\theta}}(\mathbf{X}; \psi_a))$. As MUSIC is applied here each time only to recover a single range, we can use its output as part of our loss function (instead of monitoring the spectrum directly as we did when recovering multiple source in Subsection III-A), using a differentiable approximation detailed below in the overall training algorithm.

Since each distance is associated with a specific angle, the ordering in $\hat{\rho}$ matches that in $\hat{\boldsymbol{\theta}}$. Consequently, the loss term here for an input \mathbf{X} with distances ρ is

$$l_r(\mathbf{X}, \rho; \psi_r) = \frac{\|\rho - P_{\theta} \hat{\rho}(\hat{\mathbf{R}}(\mathbf{X}; \psi_r), \hat{\boldsymbol{\theta}}(\mathbf{X}; \psi_a))\|}{\sqrt{M}}, \quad (21)$$

where P_{θ} is the angles permutation from (19). For far-field sources, the distance is the farthest edge of the search range. The overall loss over the dataset \mathcal{D} is

$$\mathcal{L}_{\mathcal{D}}^r(\psi_r) = \frac{1}{|\mathcal{D}|} \sum_{j=1}^{|\mathcal{D}|} l_r(\mathbf{X}_j, \rho_j; \psi_r). \quad (22)$$

As an initial warm-up stage, we begin training by using the ground-truth angles rather than the angles recovered from the trained ψ_a . This approach mitigates the effect of noisy angle estimates during the early stages of range recovery. After a few epochs, once the model has learned to accurately estimate the ranges, we switch to using the predicted angles for the remainder of the training process to adapt our model to yield better ranges estimation even for noisy angles.

Position Training: We conclude by jointly tuning ψ_r and ψ_a based on the Cartesian position. Let $C(\boldsymbol{\theta}, \rho)$ be the $M \times 2$ Cartesian representation of $\boldsymbol{\theta}, \rho$. The resulting position loss is

$$l_p(\mathbf{X}, \boldsymbol{\theta}, \rho; \psi_a, \psi_r) = \min_{\mathbf{P} \in \mathcal{P}_M} \frac{\|C(\boldsymbol{\theta}, \rho) - \mathbf{P}C(\hat{\boldsymbol{\theta}}, \hat{\rho})\|}{\sqrt{M}}. \quad (23)$$

The loss over \mathcal{D} used in the final training stage is

$$\mathcal{L}_{\mathcal{D}}^p(\psi_a, \psi_r) = \frac{1}{|\mathcal{D}|} \sum_{j=1}^{|\mathcal{D}|} l_p(\mathbf{X}_j, \boldsymbol{\theta}_j, \rho_j; \psi_a, \psi_r) + \mu_e l_e(\mathbf{X}_j, M_j; \psi_a). \quad (24)$$

Training Algorithm: We train DCD-MUSIC using standard deep learning methods based on SGD in the following stages:

- S1 Train ψ_a based on $\mathcal{L}_{\mathcal{D}}^a(\psi_a)$;
- S2 Train ψ_r based on $\mathcal{L}_{\mathcal{D}}^r(\psi_r)$;

S3 Further tune ψ_a and ψ_r based on $\mathcal{L}_{\mathcal{D}}^p(\psi_a, \psi_r)$.

A core challenge with this procedure stems from the fact that recovering ranges via MUSIC, i.e., $\arg \max$ of (10), is non-differentiable, limiting the usage of SGD in stages (ii) and (iii). However, as DCD-MUSIC employs one-dimensional MUSIC for recovering a single range each time, its non-differentiability can be faithfully approached using a differentiable mapping. Specifically, drawing inspiration from [65], we approximate $\arg \max$ with a differentiable *Maskpeak* when taking the gradients. Let L be the mask size. We compute the gradients approximating $\hat{\rho}_m^{\text{peak}} = \arg \max_{\rho} P_{\text{MUSIC}}(\hat{\theta}_m, \rho)$ by observing a window denoted ρ_m^{mask} over the search range of size $2L + 1$ centered at $\hat{\rho}_m^{\text{peak}}$. Then we take the gradients over the weighted sum of the masked ranges dictionary by,

$$\hat{\rho}_m = (\rho_m^{\text{mask}})^T \text{softmax} \left(P_{\text{MUSIC}}(\hat{\theta}_m, \rho_m^{\text{mask}}) \right), \quad (25)$$

with $P_{\text{MUSIC}}(\cdot)$ computed using $\hat{\mathbf{R}}(\mathbf{X}; \psi_r)$. To sharpen the approximation, L gradually decreases each epoch. We summarize the training method using mini-batch SGD as Algorithm 4.

Algorithm 4: SGD Training of DCD-MUSIC

Init : Learning parameters $(\mu, e_{\max}, B, \{L_e\})$, hyperparameters (ϵ, τ_{\max}) , initial weights ψ_a, ψ_r ;

Input : Training dataset \mathcal{D}

Stage 1: Angle Training;

```

1 for  $e = 1, \dots, e_{\max}$  do
2   Randomly divide  $\mathcal{D}$  into  $B$  batches;
3   for each batch  $\mathcal{D}^{(b)}$  do
4     Compute  $\hat{\mathbf{R}}(\mathbf{X}_j^{(b)}; \psi_a)$ ,  $\forall \mathbf{X}_j^{(b)} \in \mathcal{D}^{(b)}$ ;
5     Estimate angles using ESPRIT;
6     Compute loss  $\mathcal{L}_{\mathcal{D}^{(b)}}^a(\psi_a)$  using (20);
7     Update  $\psi_a \leftarrow \psi_a - \mu \nabla_{\psi_a} \mathcal{L}_{\mathcal{D}^{(b)}}(\psi_a)$ ;
```

Stage 2: Range Training;

```

8 for  $e = 1, \dots, e_{\max}$  do
9   Randomly divide  $\mathcal{D}$  into  $B$  batches;
10  for each batch  $\mathcal{D}^{(b)}$  do
11    Compute  $\hat{\mathbf{R}}(\mathbf{X}_j^{(b)}; \psi_r)$ ,  $\forall \mathbf{X}_j^{(b)} \in \mathcal{D}^{(b)}$ ;
12    Estimate ranges using (25) with mask  $L_e$ ;
13    Compute loss  $\mathcal{L}_{\mathcal{D}^{(b)}}^r(\psi_r)$  using (22);
14    Update  $\psi_r \leftarrow \psi_r - \mu \nabla_{\psi_r} \mathcal{L}_{\mathcal{D}^{(b)}}(\psi_r)$ ;
```

Stage 3: Position Training;

```

15 for  $e = 1, \dots, e_{\max}$  do
16   Randomly divide  $\mathcal{D}$  into  $B$  batches;
17   for each batch  $\mathcal{D}^{(b)}$  do
18     Apply Algorithm 3
       with parameters  $\psi = (\psi_a, \psi_r)$  to batch
       while replacing (18) with (25) of mask  $L_e$ ;
19     Compute loss  $\mathcal{L}_{\mathcal{D}^{(b)}}^p(\psi_a, \psi_r)$  using (24);
20     Update  $\psi \leftarrow \psi - \mu \nabla_{\psi} \mathcal{L}_{\mathcal{D}^{(b)}}(\psi)$ ;
21 return  $\psi_a, \psi_r$ 
```

C. Discussion

We introduce two AI-aided subspace methods, NF-SubspaceNet and DCD-MUSIC. Both algorithms are designed to preserve the interpretable operation of subspace-based localization, while enabling it to deal with challenges **C1-C4** via AI augmentation. To understand the individual strengths of the proposed approach, as well as their interplay with standard near-field subspace methods, we next provide a qualitative comparison, which is complemented by a quantitative evaluation reported in Section IV. In the following, we focus on the following measures: *Complexity*, *Training*, and *Favorable Properties*. The comparison is summarized as Table I.

Complexity: As our algorithms combine DNNs with subspace methods, their inference complexity is highly coupled with that of standard Near-Field MUSIC. The latter is dominated by the empirical covariance estimate (complexity of $\mathcal{O}(TN^2)$); EVD (complexity of $\mathcal{O}(N^3)$); and evaluation of the MUSIC spectrum over a grid with $G_{2D} = G_A \times G_R$ points (complexity of $\mathcal{O}(G_{2D}N^2)$). NF-SubspaceNet preserves the operation of Near-Field MUSIC, while replacing the empirical covariance with empirical autocorrelation (complexity of $\mathcal{O}(\tau TN^2)$), to which a CNN autoencoder is applied. As the number of products of a convolutional layer is proportional to its input size and the number of parameters [66], its complexity is of an order of $\mathcal{O}(CN^2)$, where the coefficient C depends on the number of DNN parameters and layers. In the likely case where $N \ll \max(G_{2D}, C, T)$, the resulting complexity is

$$\mathcal{C}_{\text{NFS}} = \mathcal{O}(N^2(\tau T + C + G_{2D})), \quad (26)$$

which is often dominated by the grid size G_{2D} .

DCD-MUSIC eliminates the need for exhaustive 2D grid searching by processing the input signal through two autoencoders, followed by the ESPRIT algorithm. Unlike MUSIC, ESPRIT solves a least squares problem and performs an M -dimensional EVD instead of peak searching, at an overall complexity order of $\mathcal{O}(NM^2)$. The final step applies 1D-MUSIC M times over the range dimension alone, using a 1D grid of G_R points. Consequently, the overall complexity order, again assuming $N \ll \max(G_R, C, T)$, is

$$\mathcal{C}_{\text{DCD}} = \mathcal{O}(N^2(\tau T + 2C + MG_R)). \quad (27)$$

Consequently, the complexity difference between NF-SubspaceNet in (26) and DCD-MUSIC in (27) depends on the selected grid sizes and the complexity of the autoencoders.

Training: Being supervised AI-aided algorithms, both NF-SubspaceNet and DCD-MUSIC require training from labeled data. While training is typically done offline, its complexity is still an important aspect. For NF-SubspaceNet, the training procedure is straightforward, and given the novel loss function in (17), it can be trained via standard deep learning methods as in Algorithm 2. The cascaded operation of DCD-MUSIC necessitates a more involved three-step training procedure as summarized in Algorithm 4, making it more complex and time-consuming to optimize compared to NF-SubspaceNet.

Favorable Properties: Being the main motivation in their formulation, both NF-SubspaceNet and DCD-MUSIC can successfully apply subspace methods in the presence of challenges

	Near-Field MUSIC	NF-SubspaceNet	DCD-MUSIC
Complexity	$\mathcal{O}(N^2(T + G_{2D}))$	$\mathcal{O}(N^2(\tau T + C + G_{2D}))$	$\mathcal{O}(N^2(\tau T + 2C + MG_R))$
Training	Not needed	Standard	3 Stages
C1-C3	Not suitable	Suitable	Suitable
Shared angles	Suitable	Suitable	Not suitable
Handle C4	Requires adaptation	At additional training	Suitable

TABLE I: Qualitative comparison summary.

C1-C3, where standard subspace methods struggle. These capabilities are numerically demonstrated in Section IV. However, each algorithm achieves these capabilities with a different structure, leading to distinct properties.

For once, DCD-MUSIC does not preserve the flow of Near-Field MUSIC, and separates angle recovery from range estimation. As a result, it cannot handle sources that share the same angle. However, the fact that it learns to compute surrogate covariance matrix under the far-field assumption, makes it well-suited for handling far-field sources and mixed near-far field scenarios (**C4**), and can achieve this capability without being trained to do so, as shown in Section IV.

While NF-SubspaceNet can also handle mixed near-field/far-field sources (**C4**), it requires dedicated training using data comprised with both far and near field sources to do so. However, the fact that it preserves the operation of Near-Field MUSIC allows it to localize users at similar angles. Moreover, its surrogate "clean" near-field covariance matrix can also be combined with alternative algorithms that require such statistical moments, e.g., generating focused beams via beamforming, as we show in Section IV.

Potential Extensions: Our AI-aided near-field localization algorithms give rise to multiple avenues for future investigation. While we focus here on localization with ULAs, our methodology can potentially extend to planar arrays, enabling 3D near-field localization [67], as well as to sparse arrays [68], leveraging data to cope with the inherent challenge in calibrating virtual array elements. Moreover, the fact that we cast near-field localization as a machine learning model facilitates its joint learning along with likely downstream processing, such as tracking [69]. This system-level perspective be potentially used to learn to provide features most useful for tracking, leverage tracking confidence for online adaptation, and even jointly learning to localize and track [70]. These extensions are all left for future study.

IV. EXPERIMENTAL STUDY

This section numerically evaluates our proposed AI-aided near-field localization algorithms. We first detail the experimental setup in Subsection IV-A. Then, we report our numerical results, evaluating estimation accuracy and the ability to generate interpretable spectra in Subsections IV-B-IV-C, respectively.

A. Experimental Setup

1) *Signal Model:* We simulate two different ULA configurations: (i) The setting used in Subsections IV-B-IV-C employs an array with $N = 15$ sensors, spaced at half the wavelength at a carrier frequency of 300 MHz; (ii) The large-scale setting evaluated in Subsection IV-B5 uses an array with $N = 64$

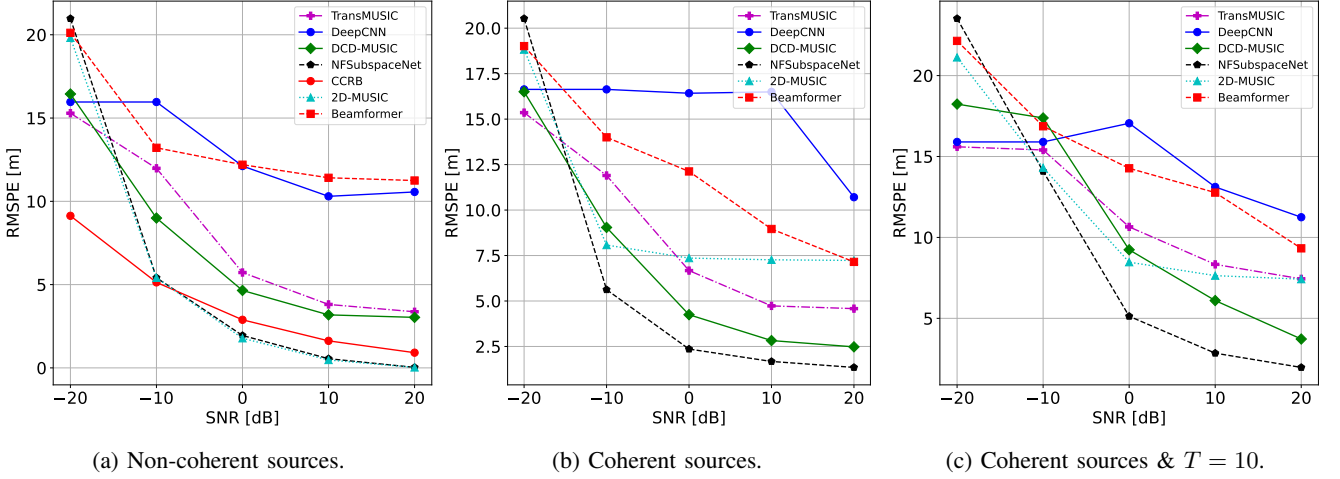


Fig. 4: RMSPE vs. SNR, $M = 2$ sources.

elements with half wavelength spacing at 5 GHz. In all settings, the sources' DoAs and ranges are uniformly drawn from $[-\frac{\pi}{3}, \frac{\pi}{3}]$ and from the Fresnel limit up to half the Fraunhofer limit, respectively. Unless stated otherwise, the trajectory length is set to $T = 100$, the array is assumed to be fully calibrated, and both the signal and noise are modeled as complex normal distributions with zero mean and unit covariance. For the coherent case, the sources transmit the same signal, creating fully correlated sources.

2) *Evaluation Metrics*: We evaluate the RMSPE of the position error, which is therefore reported in meters, under varying key parameters, including the SNR, the number of snapshots and the number of sources. Further, we assess robustness in the presence of coherent sources, and array miscalibration, where the exact locations of the sensor elements are unknown to the tested algorithms. In addition to RMSPE, we also assess the algorithms' ability to estimate the number of sources using the different suggested techniques. The interpretability of our solutions is analyzed through MUSIC spectrum and the beampattern.

3) *Localization Algorithms*: We implement NF-SubspaceNet and DCD-MUSIC using a CNN autoencoder architecture with 3 encoding and decoding convolutional layers. We compare our results to different model-based algorithms, including Near-Field MUSIC (termed *2D MUSIC*), which employs spatial smoothing (SPS) for the coherent case [71]; and standard beamforming [59]. For non-coherent cases, we also report the Conditional Cramér–Rao Bound (CCRB), using its derivation for non-coherent sources in [72]. As for data-driven benchmarks, we use the Transformer MUSIC (TransMUSIC) architecture [40] and the CNN based model suggested [73] (which we coin *DeepCNN*), adapting them to be suitable for the near-field scenario. In settings with unknown number of sources, we used AIC, MDL, or thresholding to estimate M .

All methods involving grid searching use the same resolution of 0.5° in $[-60^\circ, 60^\circ]$ and 0.5 meters between the Fresnel and half the Fraunhofer limits. Unless stated otherwise, the training dataset comprises $|\mathcal{D}| = 4096$ samples, we focus on a limited training dataset to match a real life system which labeled data is not easily obtained, and the algorithms were evaluated on a test dataset with 410 different source locations over the specified possible values above. The full details of our architecture and

training hyperparameters can be found in our GitHub repository at <https://github.com/ShlezingerLab/AI-Subspace-Methods>.

B. Estimation Accuracy

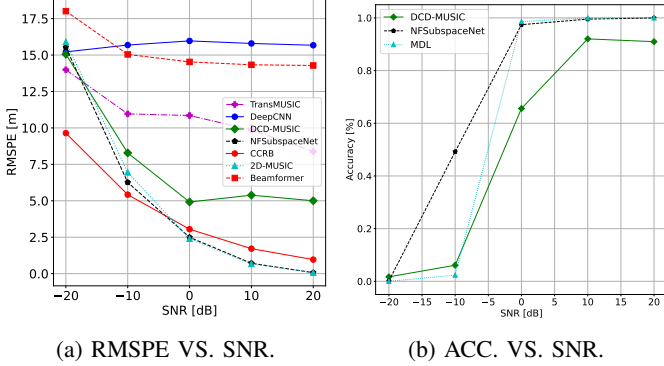
1) *Fixed Number of Sources*: Our first evaluation compares the considered localization algorithms in the case where the number of sources is fixed at $M = 2$. The RMSPE results are presented in Fig. 4 for non-coherent and coherent sources, as well as for a scenario with coherent sources and a short trajectory of only $T = 10$ samples. Fig. 4 indicates that when conditions **C1** and **C3** do not hold, 2D-MUSIC performs well, similar to data-driven approaches. However, when dealing with coherent sources or an insufficient number of snapshots, the model-based algorithm fails to localize accurately. In contrast, both NF-SubspaceNet and DCD-MUSIC demonstrate robust performance under these challenging conditions. Additionally, due to their high parameterization, both TransMUSIC and DeepCNN, struggle to generalize when trained with only 4096 samples. Specifically, DeepCNN shows superior performances only for low SNR values.

2) *Mixed Number of Sources*: We proceed to a more difficult setting in which the number of sources M varies between 2 and 8 sources, drawn uniformly for each sample in the training and test datasets. Additionally, we evaluated different regularization methods to determine which provides better localization and model order estimation for such scenarios. As a baseline, we also included a model-based method for model-order estimation. The results are presented in Table II. A key observation here is that using the model order selection test directly on the surrogate covariance yields similar results to the classic use of empirical covariance when the sources are non-coherent. For the coherent case, we can achieve up to 60 % accuracy, where the model-based approaches fail, while also achieving improved RMSPE performance. Note that the results of TransMUSIC, which uses an additional DNN for estimating M , were not included in the table due to observing a major reduction with localization performance when training the source estimation branch as suggests in [40].

Moreover, the regularization introduced to facilitate model-order selection does not necessarily degrade localization accuracy, particularly in more challenging settings with coherent sources, possibly owing to its further encouraging the surrogate

Scenario	Method	2D-MUSIC		NF-SubspaceNet		DCD-MUSIC	
		Acc.[%]	RMSPE[m]	Acc.[%]	RMSPE[m]	Acc.[%]	RMSPE[m]
Non Coherent	None	-	0.674	-	0.716	-	4.578
	MDL	100		99.5	0.712	88.6	4.654
	AIC	92.2		94	0.723	92.5	5.349
	Threshold	32.7		34.7	0.72	40.2	5.5
Coherent	None	-	13.758	-	7.665	-	10.463
	MDL	0		32	7.832	12.1	10.231
	AIC	0		58.5	7.303	48.5	10.231
	Threshold	0		34.2	7.688	27.2	10.622

TABLE II: Performance comparison of different model order estimation methods and regularization techniques.



(a) RMSPE VS. SNR.

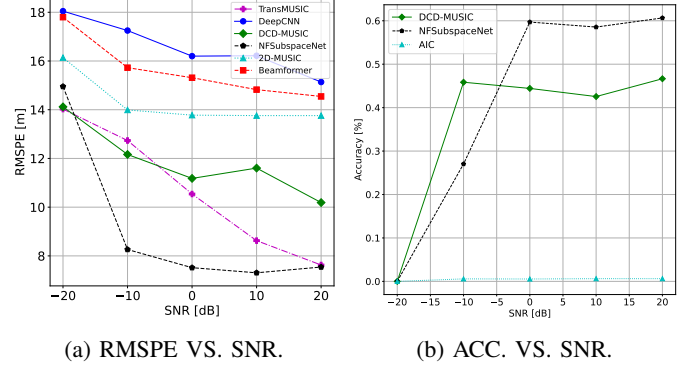
(b) ACC. VS. SNR.

Fig. 5: Mixed number of non-coherent sources.

covariance to be suitable to downstream subspace-based processing. Specifically, when considering the coherent case with AIC, NF-SubspaceNet manages to improve its localization comparing to training without any regularization.

The ability of our algorithms to simultaneously localize and identify the number of sources is further evident when evaluating these metrics in both non-coherent and fully coherent scenarios for different SNR values. In this scenario, the data size is $|\mathcal{D}| = 40,000$ and the test dataset includes 4,000 samples. The results are reported in Fig. 5 and Fig. 6. Based on the findings in Table II, we use MDL and AIC, for the non-coherent and coherent cases respectively for NF-SubspaceNet, and AIC for DCD-MUSIC, as the model order estimation method as well as the regularization term in the training stage. The results suggest that for non-coherent case, both data-driven and model-based methods successfully localize up to 8 sources, with the best performance in terms of both RMSPE and localization accuracy achieved using using NF-SubspaceNet. For the coherent case, the data-driven algorithms outperform the model-based ones, and the lowest RMSPE achieved by the NF-SubspaceNet at SNR = 20dB but with only a minor gap from TransMUSIC, that was able to localized better than DCD-MUSIC. NF-SubspaceNet and DCD-MUSIC were able to partly estimate the number of sources with up to 60% accuracy.

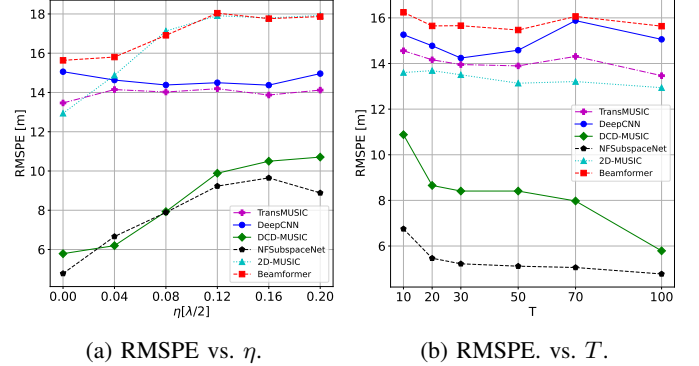
3) *Miscalibration and Limited Snapshots*: We next consider challenging settings induced by non-calibrated arrays (C2) and few snapshots (C3). The former is simulated by adding noise distributed uniformly in $[-\eta, \eta]$ to each sensor location. The simulation results for these scenarios with $M = 3$ sources at 0 dB SNR are reported in Fig. 7. Observing Fig. 7, we note that our algorithms successfully cope with miscalibrated array, with both NF-SubspaceNet and DCD-MUSIC consistently achieving the most accurate localization. We can also see that



(a) RMSPE VS. SNR.

(b) ACC. VS. SNR.

Fig. 6: Mixed number of coherent sources.

(a) RMSPE vs. η .(b) RMSPE vs. T .Fig. 7: RMSPE vs. T and η , 3 coherent sources.

the ability of NF-SubspaceNet to overcome insufficient number of snapshot, only $T = 10$.

4) *Mixed Near-Field/Far-Field Sources*: We conclude the section by considering a mixture of sources located in both near-field and far-field regions (C4). To simulate this scenario, we used the full steering vector model of a ULA, without relying on Fraunhofer or Fresnel approximations, given as [17], [21]

$$[a(\theta_m, \rho_m)]_n = e^{-j \frac{2\pi}{\lambda} \rho_m \left(1 - \sqrt{1 - 2 \cdot \frac{\lambda \cdot n}{2 \cdot \rho_m} \sin \theta_m + \left(\frac{\lambda \cdot n}{2 \cdot \rho_m}\right)^2}\right)}.$$

Sources Range	2D-MUSIC	NF-SubspaceNet	DCD-MUSIC
Fresnel : 0.5 · Fraunhofer (Fresnel approx.)	$4.527 \cdot 10^{-5}$	$5.281 \cdot 10^{-5}$	$1.347 \cdot 10^{-2}$
Fresnel : 0.5 · Fraunhofer	$5.395 \cdot 10^{-2}$	$4.154 \cdot 10^{-2}$	$1.66 \cdot 10^{-2}$
Fresnel : 1 · Fraunhofer	$1.124 \cdot 10^{-1}$	$1.739 \cdot 10^{-1}$	$1.174 \cdot 10^{-2}$
Fresnel : 2 · Fraunhofer	$2.485 \cdot 10^{-1}$	$2.75 \cdot 10^{-1}$	$1.045 \cdot 10^{-2}$
Fresnel : 5 · Fraunhofer	$3.709 \cdot 10^{-1}$	$3.811 \cdot 10^{-1}$	$9.583 \cdot 10^{-3}$
Fresnel : 10 · Fraunhofer	$3.753 \cdot 10^{-1}$	$3.708 \cdot 10^{-1}$	$9.337 \cdot 10^{-3}$

TABLE III: Angle RMSPE in radians for different ranges.

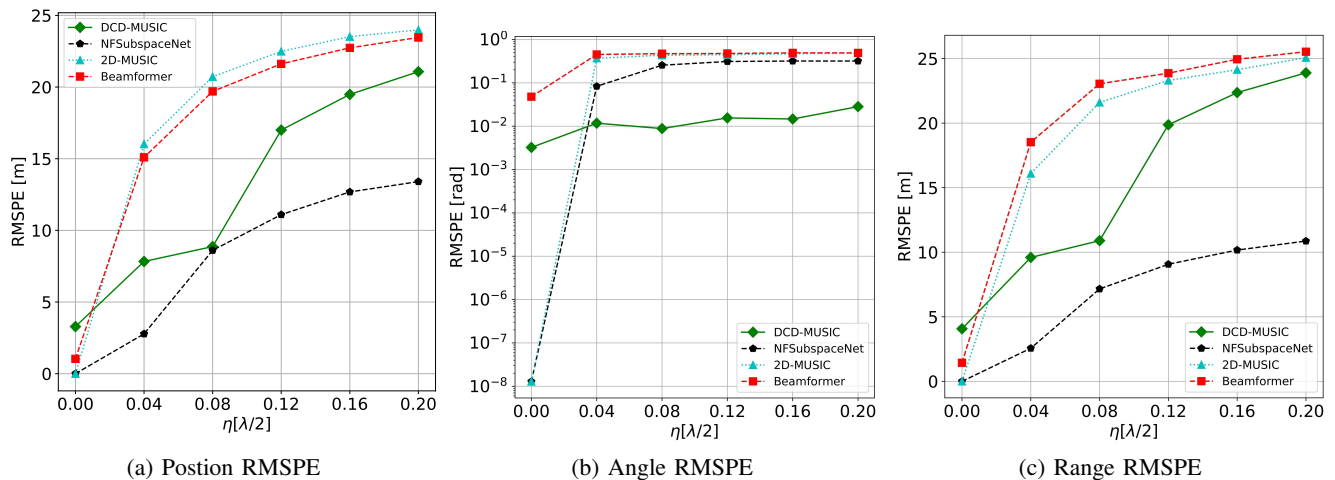


Fig. 8: RMSPE vs. Calibration error, $M = 2$ non-coherent sources.

We compare DCD-MUSIC and NF-SubspaceNet with 2D-MUSIC. All methods employ near-field approximations as in (3). The scenario consists of $M = 2$ non-coherent sources with an SNR of 20 dB. The AI-aided models were trained on data simulated using the Fresnel approximation rather than the full steering vector model. Additionally, the search grid for the range was constrained to values within the Fraunhofer limit.

The results for this setting are reported in Table III. The first two rows illustrate the differences arising from using different steering vector models for data generation. As expected, all methods exhibit some degradation in performance. When examining additional sources beyond the Fraunhofer limit, we observe that DCD-MUSIC actually improves, owing to its ability to map near-field sources into a far-field surrogate covariance matrix. In contrast, both NF-SubspaceNet and 2D-MUSIC struggle in these cases. The application of the Fresnel approximation to both near-field and far-field sources in MUSIC introduces errors due to the Taylor series residual, while NF-SubspaceNet, having been trained solely on near-field sources with the Fresnel approximation, encounters difficulties when generalizing to far-field conditions. Remarkably, DCD-MUSIC demonstrates strong performance in zero-shot inference for mixed far-field and near-field sources.

5) *Large-Scale ULA*: A key motivation for developing near-field localization algorithms arises due to the anticipated deployment of large antenna arrays [3]. To demonstrate the applicability of our method, we simulated a large-scale ULA with $N = 64$ elements and a carrier frequency of 5 GHz. In this scenario we tested the algorithms' ability to cope with calibration error (modeled as a randomized shifts in each sensor location) with SNR of 20 dB. Here, the Fresnel and Fraunhofer distances, calculated using the array diameter as per (1), result in a Fresnel distance of about 3 meters and Fraunhofer limit of about 120 meters. As this changes the range values, we use a larger dataset of size $|\mathcal{D}| = 10^5$ for training. The data-driven benchmarks failed to learn in such large scale settings from such limited data, and are thus not reported here.

The results for this scenario are presented in Fig. 8. Here, in addition to position results, we also report the individual accuracy in recovering the angle and range, to examine the

differences in methods performances. In general, we can see that DCD-MUSIC is able to easily adapt to mis-calibrated array, achieving consistent performances for different strength of calibration error. As expected, both NF-SubspaceNet and MUSIC achieve better results when the array is fully calibrated ($\eta = 0$). In addition, we can see that NF-SubspaceNet is most accurate in recovering the position, which likely follows from its capability to correctly estimate the range.

C. Interpretability

A major motivation for our usage of model-based deep learning is the desire to preserve the ability of subspace methods to provide an interpretable spectrum representation. To demonstrate this, we examine the spectrum of our methods, the 2D spectrum of NF-SubspaceNet and 1D range spectrum of DCD-MUSIC. We simulated $M = 2$ sources, with 10 dB SNR and $T = 100$ snapshots for both coherent and non coherent scenarios. In Fig. 9 and Fig. 10 we can see the spectrum for the non-coherent and coherent case respectively. Both DCD-MUSIC and NF-SubspaceNet yield meaningful spectrum even when the sources are highly correlated, unlike the model-based 2D-MUSIC. In addition, we observe that the error grows with the sources approach to the Fraunhofer limit.

In addition to observing the MUSIC spectrum, we also evaluate the usefulness of the surrogate near-field covariance produced by NF-SubspaceNet for generating focused beams. To this end, we simulate two different scenarios. In the first scenario, we consider $M = 2$ coherent sources with SNR of 10 dB, located at $(-25^\circ, 15 \text{ m})$ and $(25^\circ, 35 \text{ m})$. In the second scenario, we simulate $M = 3$ coherent sources with an SNR of 0 dB, positioned at $(-25^\circ, 15 \text{ m})$, $(25^\circ, 20 \text{ m})$, and $(-25^\circ, 40 \text{ m})$. The latter scenario is significantly more challenging due to sources sharing the same angle. The results are presented in Fig. 11 and Fig. 12 for the two-source and three-source cases, respectively. These beampatterns highlight the advantages of our model-based deep learning approach, demonstrating that the surrogate covariance is a valuable tool for various tasks, including beamforming. When comparing to the classic approach, the surrogate covariance enables a clear distinction between coherent sources, even when they share the same angle. This is evidenced by the clear beam focusing around each source. In contrast,

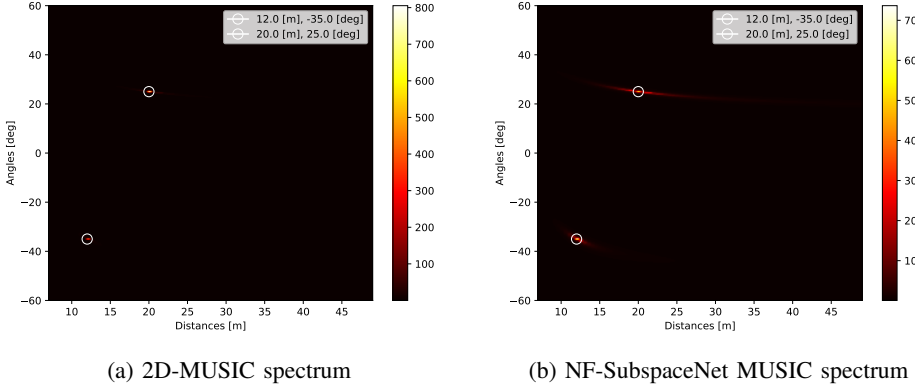


Fig. 9: MUSIC spectrum for 2 non-coherent sources, located at $(-35^\circ, 12m)$, $(25^\circ, 20m)$.

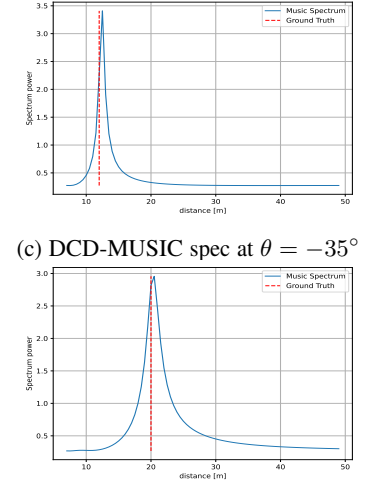
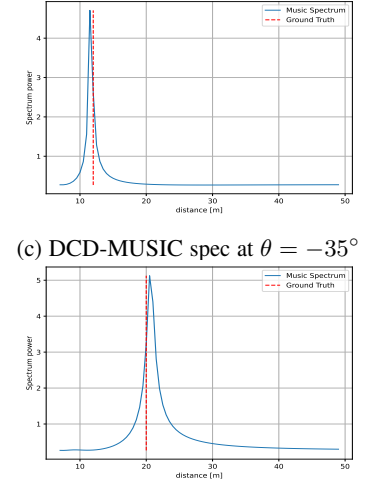
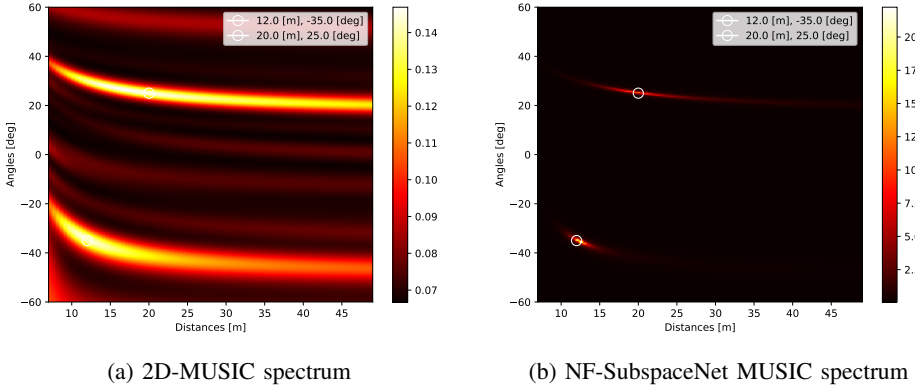


Fig. 10: spectra of 2D-MUSIC, NF-SubspaceNet and DCD-MUSIC for 2 coherent sources, located at $(-35^\circ, 12m)$, $(25^\circ, 20m)$.

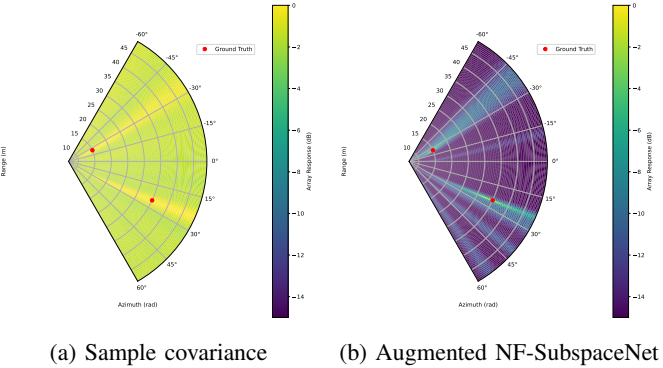


Fig. 11: Beampattern for $M = 2$ coherent sources.

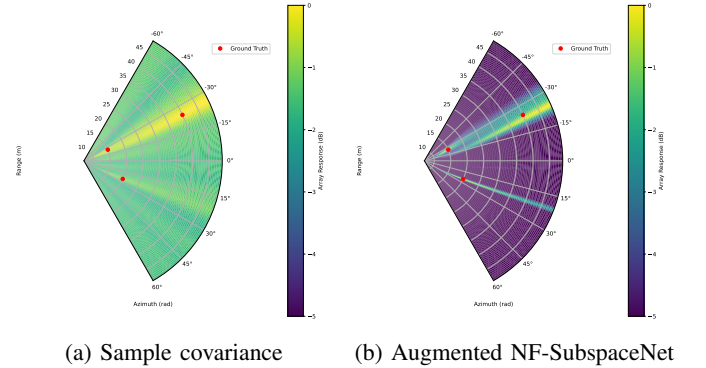


Fig. 12: Beampattern for $M = 3$ coherent sources.

using sample covariance directly for beamforming results in a more uniform energy distribution across different locations.

D. Time Complexity

We next complement the complexity analysis of Subsection III-C, and add an empirical time analysis in addition to

assessing non-asymptotic complexity by counting Multiply-Accumulate Operations (MACss). The time analysis was performed by averaging the inference time of each model over 500 trials from the setup of Fig. 4, each passed with a batch size

Model	MACs (M)	Inference Time (ms)
DCD-MUSIC	29.383	5.691
NF-SubspaceNet	14.692	15.160
DeepCNN	212.774	16.527
TransMUSIC	19.843	18.086

TABLE IV: Latency and MACs comparison

of 1. The MACs analysis was done using the THOP library¹. The simulations were run on the same CPU, without threading, over a Linux OS, and ignoring any potential acceleration that could be achieved by using GPUs. The results are shown in Table IV. We can observe that, although NF-SubspaceNet has fewer MACs operations than DCD-MUSIC, its inference time is higher due to the expensive 2D grid search involved in its architecture. Furthermore, TransMUSIC has a slower inference time despite having fewer MACs operations, likely due to the use of the Transformer architecture, which is known for being more computationally intensive in terms of memory and operation complexity.

V. CONCLUSIONS

We proposed two AI-aided subspace algorithms for near-field localization. The first algorithm, coined NF-SubspaceNet, is derived from Near-Field MUSIC, while our second algorithm, DCD-MUSIC, augments cascaded ESPRIT-MUSIC methods. We introduced dedicated training schemes for jointly assessing the usefulness of the MUSIC spectrum, the accuracy in recovering the number of sources, and localization performance. Our experimental evaluations consistently demonstrate that our AI-aided methods localize accurately in challenging settings, outperforming model-based and data-driven benchmarks.

REFERENCES

- [1] A. Gast, L. Le Magoarou, and N. Shlezinger, "DCD-MUSIC: Deep-learning-aided cascaded differentiable MUSIC algorithm for near-field localization of multiple sources," in *Proc. IEEE ICASSP*, 2025.
- [2] W. Saad, M. Bennis, and M. Chen, "A vision of 6G wireless systems: Applications, trends, technologies, and open research problems," *IEEE Netw.*, vol. 34, no. 3, pp. 134–142, 2019.
- [3] Z. Wang, J. Zhang, H. Du, D. Niyato, S. Cui, B. Ai, M. Debbah, K. B. Letaief, and H. V. Poor, "A tutorial on extremely large-scale mimo for 6G: Fundamentals, signal processing, and applications," *IEEE Commun. Surveys Tuts.*, vol. 26, no. 3, pp. 1560–1605, 2024.
- [4] C. Huang, S. Hu, G. C. Alexandropoulos, A. Zappone, C. Yuen, R. Zhang, M. Di Renzo, and M. Debbah, "Holographic MIMO surfaces for 6G wireless networks: Opportunities, challenges, and trends," *IEEE Commun. Mag.*, vol. 27, no. 5, pp. 118–125, 2020.
- [5] S. Hu, F. Rusek, and O. Edfors, "Beyond massive MIMO: The potential of data transmission with large intelligent surfaces," *IEEE Trans. Signal Process.*, vol. 66, no. 10, pp. 2746–2758, 2018.
- [6] N. Shlezinger, G. C. Alexandropoulos, M. F. Imani, Y. C. Eldar, and D. R. Smith, "Dynamic metasurface antennas for 6G extreme massive MIMO communications," *IEEE Wireless Commun.*, vol. 28, no. 2, pp. 106–113, 2021.
- [7] T. S. Rappaport, Y. Xing, O. Kanhere, S. Ju, A. Madanayake, S. Mandal, A. Alkhateeb, and G. C. Trichopoulos, "Wireless communications and applications above 100 GHz: Opportunities and challenges for 6G and beyond," *IEEE Access*, vol. 7, pp. 78 729–78 757, 2019.
- [8] W. Jiang, Q. Zhou, J. He, M. A. Habibi, S. Melnyk, M. El-Absi, B. Han, M. Di Renzo, H. D. Schotten, F.-L. Luo, T. S. El-Bawab, M. Juntti, M. Debbah, and V. C. M. Leung, "Terahertz communications and sensing for 6G and beyond: A comprehensive review," *IEEE Commun. Surveys Tuts.*, vol. 26, no. 4, pp. 2326–2381, 2024.
- [9] H. Zhang, N. Shlezinger, F. Guidi, D. Dardari, M. F. Imani, and Y. C. Eldar, "Beam focusing for near-field multiuser MIMO communications," *IEEE Trans. Wireless Commun.*, vol. 21, no. 9, pp. 7476–7490, 2022.

- [10] H. Zhang, N. Shlezinger, F. Guidi, D. Dardari, and Y. C. Eldar, "6G wireless communications: From far-field beam steering to near-field beam focusing," *IEEE Commun. Mag.*, vol. 61, no. 4, pp. 72–77, 2023.
- [11] H. Lu, Y. Zeng, C. You, Y. Han, J. Zhang, Z. Wang, Z. Dong, S. Jin, C.-X. Wang, T. Jiang, X. You, and R. Zhang, "A tutorial on near-field XL-MIMO communications towards 6G," *IEEE Commun. Surveys Tuts.*, vol. 26, no. 4, pp. 2213–2257, 2024.
- [12] A. Elzanaty, A. Guerra, F. Guidi, D. Dardari, and M.-S. Alouini, "Toward 6G holographic localization: Enabling technologies and perspectives," *IEEE Internet of Things Magazine*, vol. 6, no. 3, pp. 138–143, 2023.
- [13] Q. Yang, A. Guerra, F. Guidi, N. Shlezinger, H. Zhang, D. Dardari, B. Wang, and Y. C. Eldar, "Near-field localization with dynamic metasurface antennas," in *Proc. IEEE ICASSP*, 2023.
- [14] C. Cheng, S. Liu, H. Wu, and Y. Zhang, "An efficient maximum-likelihood-like algorithm for near-field coherent source localization," *IEEE Trans. Antennas Propag.*, vol. 70, no. 7, pp. 6111–6116, 2022.
- [15] K. Hu, S. P. Chepuri, and G. Leus, "Near-field source localization using sparse recovery techniques," in *Proc. IEEE SPCOM*, 2014.
- [16] O. Rinchi, A. Elzanaty, and M.-S. Alouini, "Compressive near-field localization for multipath RIS-aided environments," *IEEE Commun. Lett.*, vol. 26, no. 6, pp. 1268–1272, 2022.
- [17] C. Guanghui, Z. Xiaoping, J. Shuang, Y. Anning, and L. Qi, "High accuracy near-field localization algorithm at low SNR using fourth-order cumulant," *IEEE Commun. Lett.*, vol. 24, no. 3, pp. 553–557, 2020.
- [18] R. Challa and S. Shamsunder, "High-order subspace-based algorithms for passive localization of near-field sources," in *Asilomar Conference on Signals, Systems and Computers*, vol. 2, 1995, pp. 777–781 vol.2.
- [19] Y. Sun, K. Ho, T. Xing, Y. Yang, and L. Chen, "Projection-based algorithm and performance analysis for TDOA localization in MPR," *IEEE Trans. Signal Process.*, vol. 72, pp. 896–911, 2024.
- [20] Y.-D. Huang and M. Barkat, "Near-field multiple source localization by passive sensor array," *IEEE Trans. Antennas Propag.*, vol. 39, no. 7, pp. 968–975, 1991.
- [21] W. Zuo, J. Xin, N. Zheng, H. Ohmori, and A. Sano, "Subspace-based near-field source localization in unknown spatially nonuniform noise environment," *IEEE Trans. Signal Process.*, vol. 68, pp. 4713–4726, 2020.
- [22] X. Zhang, W. Chen, W. Zheng, Z. Xia, and Y. Wang, "Localization of near-field sources: A reduced-dimension MUSIC algorithm," *IEEE Commun. Lett.*, vol. 22, no. 7, pp. 1422–1425, 2018.
- [23] J. Liang and D. Liu, "Passive localization of mixed near-field and far-field sources using two-stage MUSIC algorithm," *IEEE Trans. Signal Process.*, vol. 58, no. 1, pp. 108–120, 2010.
- [24] W. Zhi and M. Y.-W. Chia, "Near-field source localization via symmetric subarrays," in *Proc. IEEE ICASSP*, 2007.
- [25] D. Starer and A. Nehorai, "Passive localization of near-field sources by path following," *IEEE Trans. Signal Process.*, vol. 42, no. 3, pp. 677–680, 1994.
- [26] Z. Ebadi, A. M. Molaei, G. C. Alexandropoulos, M. A. B. Abbasi, S. Cotton, A. Tukmanov, and O. Yurduseven, "Near-field localization with antenna arrays in the presence of direction-dependent mutual coupling," *IEEE Trans. Veh. Technol.*, 2025, early access.
- [27] R. Schmidt, "Multiple emitter location and signal parameter estimation," *IEEE Trans. Antennas Propag.*, vol. 34, no. 3, pp. 276–280, 1986.
- [28] C. Chen, B. Wang, C. X. Lu, N. Trigoni, and A. Markham, "A survey on deep learning for localization and mapping: Towards the age of spatial machine intelligence," *arXiv preprint arXiv:2006.12567*, 2020.
- [29] M. Chen, Y. Gong, and X. Mao, "Deep neural network for estimation of direction of arrival with antenna array," *IEEE Access*, vol. 8, pp. 140 688–140 698, 2020.
- [30] J. Cong, X. Wang, M. Huang, and L. Wan, "Robust DOA estimation method for MIMO radar via deep neural networks," *IEEE Sensors J.*, vol. 21, no. 6, pp. 7498–7507, 2021.
- [31] Y. Cao, T. Lv, Z. Lin, P. Huang, and F. Lin, "Complex ResNet aided DoA estimation for near-field MIMO systems," *IEEE Trans. Veh. Technol.*, vol. 69, no. 10, pp. 11 139–11 151, 2020.
- [32] G. K. Papageorgiou, M. Sellathurai, and Y. C. Eldar, "Deep networks for direction-of-arrival estimation in low SNR," *IEEE Trans. Signal Process.*, vol. 69, pp. 3714–3729, 2021.
- [33] L. Wu, Z.-M. Liu, and Z.-T. Huang, "Deep convolution network for direction of arrival estimation with sparse prior," *IEEE Signal Process. Lett.*, vol. 26, no. 11, pp. 1688–1692, 2019.
- [34] H. Lee, Y. Kim, S. Seol, and J. Chung, "Deep learning-based near-field source localization without a priori knowledge of the number of sources," *IEEE Access*, vol. 10, pp. 55 360–55 368, 2022.
- [35] Y. Qin, "Deep networks for direction of arrival estimation with sparse prior in low SNR," *IEEE Access*, vol. 11, pp. 44 637–44 648, 2023.

¹<https://pypi.org/project/thop/>

- [36] Z. Jiang, J. Xin, W. Zuo, N. Zheng, and A. Sano, "Deep residual learning based localization of near-field sources in unknown spatially colored noise fields," in *Proc. IEEE EUSIPCO*, 2022.
- [37] F. Weißer, M. Baur, and W. Utschick, "Unsupervised parameter estimation using model-based decoder," in *Proc. IEEE SPAWC*, 2023, pp. 571–575.
- [38] X. Su, P. Hu, Z. Liu, T. Liu, B. Peng, and X. Li, "Mixed near-field and far-field source localization based on convolution neural networks via symmetric nested array," *IEEE Trans. Veh. Technol.*, vol. 70, no. 8, pp. 7908–7920, 2021.
- [39] X. Lan, H. Zhai, and Y. Wang, "A novel DOA estimation of closely spaced sources using attention mechanism with conformal arrays," *IEEE Access*, vol. 11, pp. 44 010–44 018, 2023.
- [40] J. Ji, W. Mao, F. Xi, and S. Chen, "TransMUSIC: A transformer-aided subspace method for DOA estimation with low-resolution ADCs," in *Proc. IEEE ICASSP*, 2024.
- [41] N. Shlezinger and Y. C. Eldar, "Model-based deep learning," *Foundations and Trends® in Signal Processing*, vol. 17, no. 4, pp. 291–416, 2023.
- [42] D. T. Hoang and K. Lee, "Deep learning-aided coherent direction-of-arrival estimation with the FTMR algorithm," *IEEE Trans. Signal Process.*, vol. 70, pp. 1118–1130, 2022.
- [43] A. M. Elbir, "DeepMUSIC: Multiple signal classification via deep learning," *IEEE Sensors Letters*, vol. 4, no. 4, pp. 1–4, 2020.
- [44] A. Barthelme and W. Utschick, "DoA estimation using neural network-based covariance matrix reconstruction," *IEEE Signal Process. Lett.*, vol. 28, pp. 783–787, 2021.
- [45] X. Wu, X. Yang, X. Jia, and F. Tian, "A gridless DOA estimation method based on convolutional neural network with Toeplitz prior," *IEEE Signal Process. Lett.*, vol. 29, pp. 1247–1251, 2022.
- [46] Z. Jiang, J. Xin, W. Zuo, N. Zheng, and A. Sano, "A Toeplitz prior-based deep learning framework for DOA estimation with unknown mutual coupling," in *Proc. EUSIPCO*, 2023, pp. 1544–1548.
- [47] J. P. Merkofer, G. Revach, N. Shlezinger, and R. J. Routtenberg, Tirza an van Sloun, "Data-driven DoA estimation via deep augmented MUSIC algorithm," *IEEE Trans. Veh. Technol.*, vol. 73, no. 2, pp. 2771–2785, 2024.
- [48] X. Xu and Q. Huang, "MD-DOA: A model-based deep learning DOA estimation architecture," *IEEE Sensors J.*, vol. 24, no. 12, pp. 20 240–20 253, 2024.
- [49] D. H. Shmuel, J. P. Merkofer, G. Revach, R. J. Van Sloun, and N. Shlezinger, "SubspaceNet: Deep learning-aided subspace methods for DoA estimation," *IEEE Trans. Veh. Technol.*, vol. 74, no. 3, pp. 4962–4976, 2025.
- [50] B. Chatelier, J. M. Mateos-Ramos, V. Corlay, C. Häger, M. Crussiere, H. Wymeersch, and L. L. Magoarou, "Physically parameterized differentiable MUSIC for DoA estimation with uncalibrated arrays," *arXiv preprint arXiv:2411.15144*, 2024.
- [51] J. Rissanen, "Modeling by shortest data description," *Automatica*, vol. 14, no. 5, pp. 465–471, 1978.
- [52] H. Akaike, "Information theory and an extension of the maximum likelihood principle," in *Selected papers of Hirotugu Akaike*. Springer, pp. 199–213.
- [53] K. T. Selvan and R. Janaswamy, "Fraunhofer and Fresnel distances: Unified derivation for aperture antennas," *IEEE Antennas Propag. Mag.*, vol. 59, no. 4, pp. 12–15, 2017.
- [54] S. U. Pillai, *Array signal processing*. Springer, 2012.
- [55] B. Friedlander, "Localization of signals in the near-field of an antenna array," *IEEE Trans. Signal Process.*, vol. 67, no. 15, pp. 3885–3893, 2019.
- [56] M. Wax and T. Kailath, "Detection of signals by information theoretic criteria," *IEEE Trans. Acoust., Speech, Signal Process.*, vol. 33, no. 2, pp. 387–392, 1985.
- [57] A. J. Barabell, "Improving the resolution performance of eigenstructure-based direction-finding algorithms," in *Proc. IEEE ICASSP*, 1983.
- [58] R. Roy and T. Kailath, "ESPRIT-estimation of signal parameters via rotational invariance techniques," *IEEE Trans. Acoust., Speech, Signal Process.*, vol. 37, no. 7, pp. 984–995, 1989.
- [59] P. Stoica, R. L. Moses *et al.*, *Spectral analysis of signals*. Pearson Prentice Hall Upper Saddle River, NJ, 2005, vol. 452.
- [60] L. Le Magoarou, A. Le Calvez, and S. Paquelet, "Massive MIMO channel estimation taking into account spherical waves," in *Proc. IEEE SPAWC*, 2019.
- [61] B. Luijten, R. Cohen, F. J. de Bruijn, H. A. W. Schmeitz, M. Mischi, Y. C. Eldar, and R. J. G. van Sloun, "Adaptive ultrasound beamforming using deep learning," *IEEE Trans. Med. Imag.*, vol. 39, no. 12, pp. 3967–3978, 2020.
- [62] N. Shlezinger and T. Routtenberg, "Discriminative and generative learning for linear estimation of random signals [lecture notes]," *IEEE Signal Process. Mag.*, vol. 40, no. 6, pp. 75–82, 2023.
- [63] O. Solomon, R. Cohen, Y. Zhang, Y. Yang, Q. He, J. Luo, R. J. van Sloun, and Y. C. Eldar, "Deep unfolded robust PCA with application to clutter suppression in ultrasound," *IEEE Trans. Med. Imag.*, vol. 39, no. 4, pp. 1051–1063, 2019.
- [64] T. Routtenberg and J. Tabrikian, "Bayesian parameter estimation using periodic cost functions," *IEEE Trans. Signal Process.*, vol. 60, no. 3, pp. 1229–1240, 2011.
- [65] J. M. Mateos-Ramos, C. Häger, M. F. Keskin, L. Le Magoarou, and H. Wymeersch, "Model-based end-to-end learning for multi-target integrated sensing and communication under hardware impairments," *IEEE Trans. Wireless Commun.*, 2025, early access.
- [66] P. Freire, S. Srivallapanondh, B. Spinnler, A. Napoli, N. Costa, J. E. Prilepsky, and S. K. Turitsyn, "Computational complexity optimization of neural network-based equalizers in digital signal processing: a comprehensive approach," *J. Lightw. Technol.*, vol. 42, no. 12, pp. 4177–4201, 2024.
- [67] S. Chen, J. Gu, W. Duan, L. Zhang, S. Dang, M. Wen, Z. Ding, and P.-H. Ho, "Near-field communications: Shape and structure design for uniform planar array," *IEEE Internet Things J.*, 2025, early access.
- [68] P. P. Vaidyanathan and P. Pal, "Sparse sensing with co-prime samplers and arrays," *IEEE Trans. Signal Process.*, vol. 59, no. 2, pp. 573–586, 2010.
- [69] A. Guerra, F. Guidi, D. Dardari, and P. M. Djurić, "Near-field tracking with large antenna arrays: Fundamental limits and practical algorithms," *IEEE Trans. Signal Process.*, vol. 69, pp. 5723–5738, 2021.
- [70] I. Buchnik, G. Revach, D. Steger, R. J. Van Sloun, T. Routtenberg, and N. Shlezinger, "Latent-KalmanNet: Learned kalman filtering for tracking from high-dimensional signals," *IEEE Trans. Signal Process.*, vol. 72, p. 367, 2023.
- [71] H. Wang, K. R. Liu, and H. Anderson, "Spatial smoothing for arrays with arbitrary geometry," in *Proc. IEEE ICASSP*, 1994.
- [72] M. N. El Korso, R. Boyer, A. Renaux, and S. Marcos, "Conditional and unconditional Cramér–Rao bounds for near-field source localization," *IEEE Trans. Signal Process.*, vol. 58, no. 5, pp. 2901–2907, 2010.
- [73] G. K. Papageorgiou, M. Sellathurai, and Y. C. Eldar, "Deep networks for direction-of-arrival estimation in low snr," *IEEE Transactions on Signal Processing*, vol. 69, pp. 3714–3729, 2021.